Graphene at fluidic interfaces

Belyaeva, L.A.

CHAPTER 6

Macroscopic and microscopic wettability of graphene: substrate effect

Interactions between water and graphene can be probed on a macroscopic level through wettability by measuring water contact angle, and on microscopic level through water desorption kinetics studies using surface science methods. Contact angle studies of graphene pinpointed the critical role of sample preparation and measurement conditions for assessing the wettability of graphene. So far, studies of water desorption from graphene under the conditions of ultra-high vacuum provided superior control over the environment, but disregarded the importance of sample preparation. In this chapter the effect of the morphology of the growth substrate and of transfer process on the macroscopic and microscopic wettability of graphene is systematically examined. Remarkably, macroscopic wetting transparency of graphene does not always translate into microscopic wetting transparency, particularly in the case of atomically-defined Cu(111) substrate. Additionally, subtle differences in substrates significantly alter the interactions between graphene and the first monolayer of adsorbed water, but have negligible effect on the apparent macroscopic wettability.

Manuscript in preparation. L.A. Belyaeva, C. Tong, G.F. Schneider, L. Juurlink

6.1. Introduction

The subject of wettability of graphene has been widely studied, but nontheless, remains under ongoing debate.[1,2] Understanding and taking control of the wetting behavior of graphene would benefit to the wide range of graphene applications – sensors, nanoelectronics, fuel cells etc.[3–8] However, there exist a remarkable discrepancy of the reported contact angles of graphene, varying from very hydrophilic when supported by water,[9] mildly hydrophilic on glass[10] to hydrophobic on silicon carbide and copper.[11,12] In general, three factors determine the wetting properties of graphene: the intrinsic wettability of graphene, the effect of the underlying substrate, i.e. the wetting transparency of graphene,[10,13,14] and the sample preparation-related environmental factors, such as morphological features and defects caused by the growth and transfer proccesses,[15] contamination and adsorption of airborne hydrocarbons.[16] And while the intrinsic contact angle of clean free-standing graphene has been already determined to be 42°±3° both theoretically[17,18] and experimentally,[19] the effects of wetting transparency and imperfections linked to performing measurements under ambient conditions are difficult to disentangle. As a result of the diversity of growth and handling conditions, graphene has been independently shown to be fully transparent,[10] partially transparent[14] and fully opaque to wetting.[11,20] Particularly, irredularities in graphene structure caused by the transfer appear paramount for the disruption of the wetting transparency.[9]

Another route to approach the wettability of graphene is to study water desorption using surface science methods, such as temperature programmed desorption (TPD)[21] and thermal desorption spectroscopy (TDS).[22,23] Contrarily to the macroscopic contact angle measurements in ambient atmosphere, TPD and TDS probe interactions between a surface and isolated water molecules under ultra high vacuum (UHV) conditions and characterize the so called “wettability on a molecular level”. The wettability on a molecular level, however, does not neccessarilly correlate with the apparent macroscopic wettability (e.g. in the case of silver and gold), but complements the macroscopic observations. Macroscopic wettability observed in ambient atmosphere involves significantly larger number of collisions and interactions between molecules (both of water and environment) than microsopic wettability observed in UHV. [24] As for studies involving contact angle measurements, several TPD and TDS studies of graphene

showed contrasting results on the wetting transparency (on molecular level) of graphene, particularly, graphene on Ru(0001), Cu and Si/SiO_2 ,were shown to be opaque in water desorption measuremets,[22,23,25] but nearly transparent in the benzene desorption measurements (with the exception of graphene on Ru(0001) which was opaque in both cases).[26] A theoretical study also demonstrated the prominent substrate effect on the water desorption on graphene by investigating the electronic properties of graphene upon water adsorption.[27] Given the extreme accuracy and cleanness of the measurements under UHV, the reported discrepancies in microscopic wettability of graphene distinctly point at the crucial role of the sample preparation preceding the desorption experiments.

Here the effects of substrate crystallinity and of transfer process on the wettability and wetting transparency of graphene were studied both from macroscopic and microscopic perspectives. The same samples were used for contact angle measurements and TPD allowing, therefore, for a direct comparison between macroscopic wettability and water desorption in vacuum. Although graphene manifests nearly wetting transparent macroscopically regardless preceding treatment, desorption measurements showed that the morphology of the substrate and transfer-induced irregularities significantly alter interactions between graphene and the first monolayer of water molecules.

6.2. Results

Three different samples were studied comparatively by contact angle measurements and TPD: i) graphene as-grown on Cu(111), ii) graphene as-grown on polycrystalline copper and iii) graphene transferred to a polycrystalline copper substrate. The bare polycrystalline copper and Cu(111) were also tested after the graphene layer was removed by argon sputtering in UHV. The as-grown samples were prepared using chemical vapor deposition (CVD) method and the transferred sample was first grown on a different copper foil according to the same CVD protocol and then transferred to polycrystalline copper using the PMMA-assisted transfer method (see Appendix 5 for more details). Then the samples were studied using TPD at various water coverages on graphene. After each measurement, the graphene layer was removed directly in the UHV

chamber by sputtering, and water desorption from the bare copper substrates was also studied using the same procedures (see Appendix 5). As copper quickly oxidizes once exposed to air, contact angles were measured for bare copper crystals after annealing in hydrogen atmosphere (i.e. within 1-2 minutes) and 30 minutes after the annealing. No oxide layer was formed in the samples of as-grown graphene on copper, as during CVD graphene grows on copper directly in vacuum without exposure to air. However, to remove the adsorbed airborne hydrocarbons[16] all graphene samples were also annealed right before contact angle measurements.

6.2.1. Graphene grown on Cu(111)

Figure 6.1a, b show that graphene grown on Cu(111) is not fully transparent to water desorption. Specifically, although graphene on Cu(111) and bare Cu(111) show the same onset desorption temperature T_{onset} close to 160K, their kinetic characteristics differ significantly. Shared leading edge and shift to higher temperatures with the increase in coverage in Figure 6.1a indicate a zero-order desorption in the case of graphene on Cu(111); and the mixed features of the zero and first order in Figure 6.1 b indicate a fractional order (between 0 and 1) desorption for bare Cu(111). The zero-order kinetics in the case of graphene on Cu(111) is ascribed to two-dimensional equilibrium between individual water molecules and islands of condensed water[21,28] and, thus, indicates that water tends to form multilayer clusters rather than continuous monolayer on graphene. Contrastingly, the fractional kinetic order of the bare Cu(111) shows that its surface is more favorable (compared to graphene on Cu(111)) for the adsorption of water molecules.

Remarkably, the adsorbed water forms different crystalline phases on graphene on Cu(111) and bare Cu(111). The desorption curves of graphene on Cu(111) display a “bump” on their descending edge (Figure 1a), indicative of the formation of the metastable amorphous water ice,[21,29–31] while the shape of the desorption curves for bare Cu(111) suggests formation of thermodynamically stable crystalline water ice.

Raman spectra in Figure 6.1c confirmed that graphene is monolayer with a sharp 2D mode and high quality with very small defect-related D mode. The absence of graphene bands in Figure 6.1d indicates that graphene was completely removed from copper after argon sputtering .

As seen from Figure 6.1e, f, the contact angle measurements did not show a significant difference between graphene on Cu(111) and bare Cu(111): 90°±1° for graphene grown on Cu(111)(Figure 6.1e) and 76°±3° for bare nonoxidized Cu(111)(Figure 6.1f). However, the slightly more hydrophobic behavior of graphene on Cu(111) coincides with its lower affinity to water on a molecular level observed in TPD.

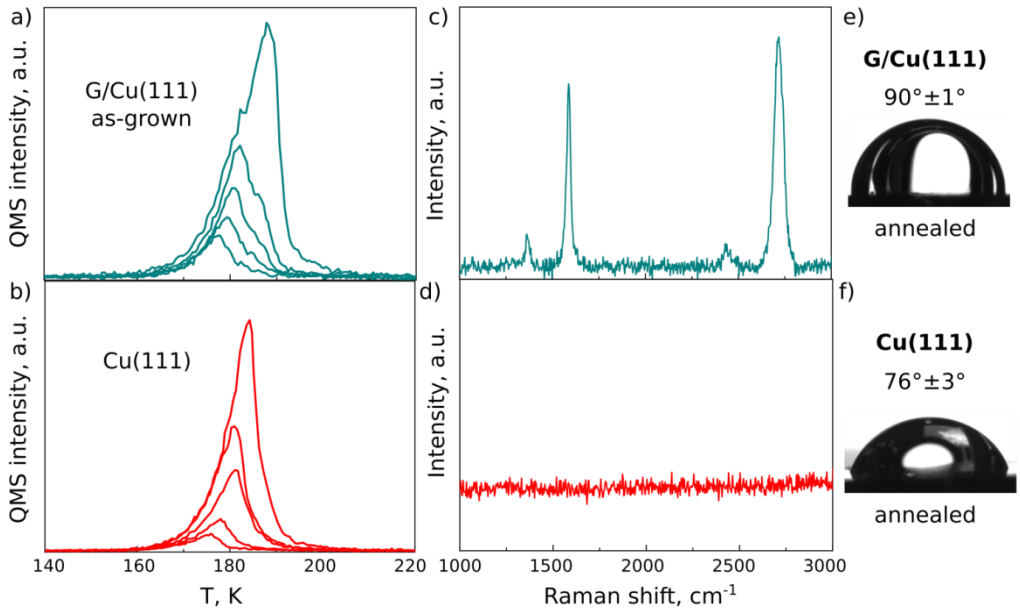

Figure 6.1. Microscopic and macroscopic wettability of graphene grown on Cu(111). a) TPD curves of graphene grown on Cu(111) at submonolayer coverages. b) Temperature programmed desorption (TPD) curves of bare Cu(111) at submonolayer coverages. c) Typical Raman spectrum of graphene grown on Cu(111). d) Typical Raman spectrum of bare Cu(111) after graphene removal by argon sputtering. e) Water contact angle of graphene grown on Cu(111) measured immediately after annealing. f) Water contact angle of Cu(111) measured immediately after annealing.

6.2.2. Graphene as-grown on polycrystalline Cu

Unlike graphene on Cu(111), graphene grown on polycrystalline copper is transparent to water desorption (Figure 6.2). The water desorption curves from graphene as-grown on polycrystalline copper and bare copper (Figure 6.2a and b respectively) display the same onset temperature T_{onset}, at 160K (also equal to that of graphene on Cu (111) and bare Cu(111)). The desorption curves show similar shapes with overlapping leading edges. This behavior is representative of zero-order desorption kinetics.[21,28] Interestingly, the shapes of the TPD curves (no "bump" on the leading edges) suggest that water forms a crystalline state on graphene on polycrystalline Cu and bare polycrystalline Cu, as opposed to amorphous in the case of graphene on Cu(111).

Contact angle measurements, on the other hand, showed that bare and graphene-coated polycrystalline copper substrates have similar contact angles (74°±1° and 85°±1° respectively, Figure 6.2e and f), suggesting that graphene is nearly transparent macrosocpically when grown on polycrystalline copper. Interestingly, the equality of the T_{onset}=160K for the polycrystalline Cu and Cu(111) is consistent with the equality of their contact angles (i.e., 74°±1° for annealed polycrystalline copper and 76°±3° for annealed Cu(111), Figure 6.2f and Figure 6.1f respectively).

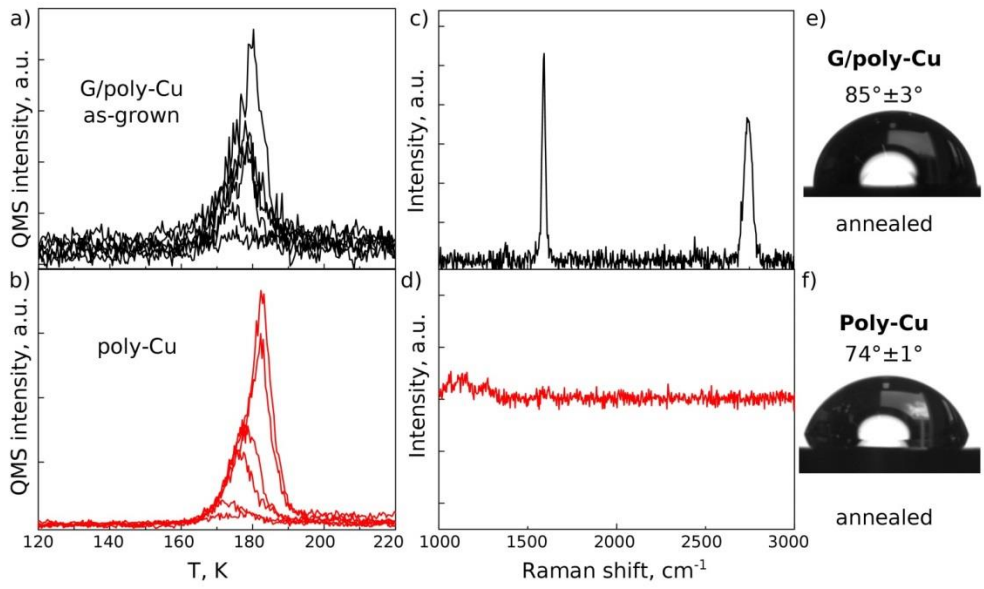

Figure 6.2. Microscopic and macroscopic wettability of graphene grown on polycrystalline Cu. a) TPD curves of graphene grown on polycrystalline Cu at submonolayer coverages. b) TPD curves of bare polycrystalline Cu at submonolayer coverages. c) Typical Raman spectrum of graphene grown on polycrystalline Cu. d) Typical Raman spectrum of bare polycrystalline Cu after graphene removal. e) Water contact angle of graphene grown on polycrystalline Cu measured right after annealing. f) Water contact angle of polycrystalline Cu measured right after annealing.

Clearly, relationships between microscopic and macroscopic wettability of graphene are not straightforward and are difficult to decipher. On one hand, the TPD was more sensitive to the morphology of the growth substrate (Cu(111) versus polycrystalline copper) and demonstrated that the morphology of the copper affects the interactions between the first layer of adsorbed water molecules and graphene, while the contact angle measurements showed no difference for graphene on Cu(111) and on polycrystalline copper (slight increase of the contact angle by ~10° as compared to the bare substrates). On the other hand, in the case of graphene on polycrystalline copper, the contact angle measurements indicated a difference in the wetting of graphene on copper and of bare copper (Figure 6.2e and f), while the desorption measurements did not detect any difference in kinetics between the two samples.

6.2.3. Graphene transferred onto polycrystalline copper

Graphene transferred onto the same polycrystalline copper, on one hand, similarly manifests wetting transparent at a molecular level, showing no difference in desorption behavior between graphene on copper and bare copper (Figure 6.3a, b). On the other hand, the TPD curves in this case exhibit different kinetic features compared to the as-grown sample: the T_{onset} of 140K and a fractional kinetic order of desorption between zero and one (shift to a higher temperature range with increasing coverage but an ascending leading edge, Figure 6.3a, b). The surprising difference in T_{onset} and kinetics even between two, in principle, identical bare copper substrates in Figure 6.2 and Figure 6.3 can be explained by the formation of copper oxide on the top copper layer in the case when graphene was trasnferred.[32] During the transfer proccess the copper crystal is inevitably exposed to air and immersed in water, which are factors that are known to cause the oxidation of copper.[33] In the case of the as-grown graphene, the copper crystal is pre-annealed in hydrogen for three hours and then immediately followed by the graphene growth in vacuum, without any exposure to the ambient oxygen. For transferred samples, therefore, the contact angle of oxidized, i.e. exposed to air, copper crystal must be measured for appropriate referencing with TPD results. Similarly to the as-grown sample, the contact angle of the graphene transferred onto Cu crystal (91°±5°, Figure 6.3e) is close to the 83°±2° of the oxidized copper crystal after exposure to air (Figure 6.3f). Interestingly, these values are higher than the 74°±1° measured for freshly-annealed copper (Figure 6.2f), which together with the lower T_{onset} of the desorption peaks (Figure 6.3a, b) indicate a more hydrophobic behavior for graphene transferred onto (oxidized) copper and bare (oxidized) copper compared to the as-grown sample and non-oxidized copper.

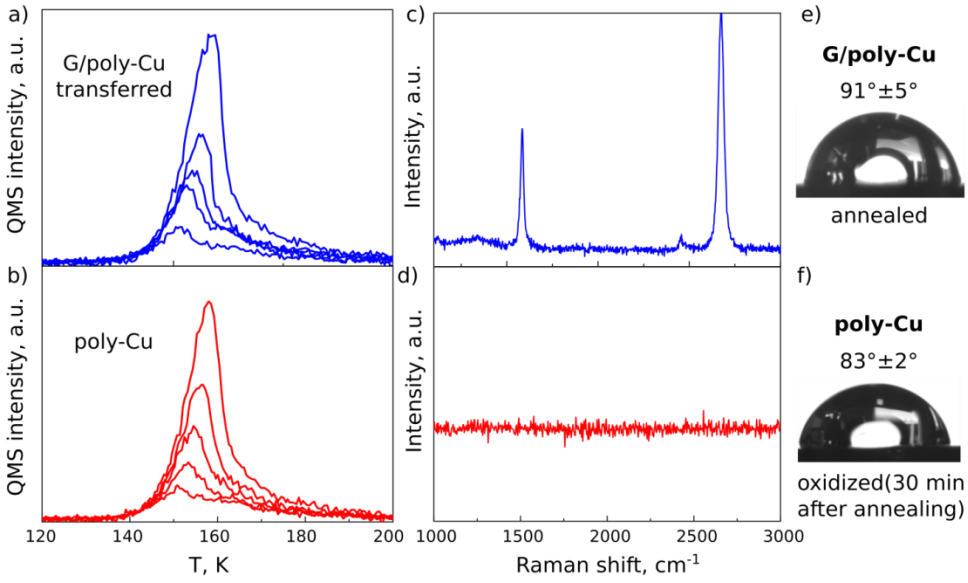

Figure 6.3. Microscopic and macroscopic wettability of graphene transferred on polycrystalline Cu. a) TPD curves of graphene transferred on polycrystalline Cu at submonolayer coverages. b) TPD curves of bare polycrystalline Cu after graphene removal at submonolayer coverages. c) Typical Raman spectrum of graphene transferred on polycrystalline Cu. d) Typical Raman spectrum of bare polycrystalline Cu after graphene removal. e) Water contact angle of graphene transferred on polycrystalline Cu measured immediately after annealing. f) Water contact angle of oxidized polycrystalline Cu measured 30 minutes after annealing.

6.3. Conclusions

In summary, the effects of substrate crystallinity and of transfer process on the interactions between graphene and water were investigated from both a microscopic and a macroscopic perspectives. Contact angle measurements showed that the macroscopic wettability of graphene is independent of the substrate crystallinity and transfer, and addition of graphene layer on top of copper only slightly increases the contact angle by ~10°, indicating that graphene is nearly wetting transparent in all three samples. Contrastingly, desorption measurements demonstrated that the morphology of the substrate and transfer-

related imperfections appreciably affect the adsorption of the water monolayer on the graphene surface. In the case of smooth and atomically-defined Cu(111), the deposition of a graphene layer not only resulted in the change of water desorption kinetics, but also in the formation of metastable amorphous water ice, as opposed to crystalline ice in the case of bare Cu(111). For rougher polycrystalline copper, on the other hand, the deposition of the graphene layer (both by direct growth and transfer) did not alter the kinetic characteristics of the copper, manifesting, therefore, wetting transparency on a molecular level. Interestingly, annealed and oxidized polycrystalline copper crystals have different desorption characteristics (T_{onset} and desorption order, see Figure 6.2b and Figure 6.3b) which are completely retained after the deposition of the graphene layer on top. The difference in wettability of as-grown and transferred graphene, observed in this work and elsewhere, therefore, seems to stem from the fact that copper is inevitably oxidized in the case of transferred graphene.

As a conclusion, the TPD and contact angle data describe different phenomena and are not perfectly intercorrelated, but rather provide complementary insights. Suchwise, due to the extreme smoothness and homogeneity of the surface of monocrystalline Cu(111), its microscopic wetting properties are readily affected by the addition of a graphene layer, while in the case of polycrystalline copper the surface properties are dominated by its significant roughness and the addition of graphene – a monoatomic and fully conforming layer – has a negligible effect. The TPD proves very sensitive to the subtle changes in the graphene and the underlying substrate (such as crystallinity) and is informative in the scenarios when interactions between graphene and individual molecules of adsorbate are of interest. Macroscopic wettability measured by contact angle measurements, on the other hand, cannot predict the interactions with individual molecules, but, instead, characterizes the interactions between graphene and macroscopic phases of adsorbate under ambient pressures. Following up the recent studies on the effect of sample preparation on the macroscopic wettability of graphene, this chapter goes further and provides more detailed insights on how different aspects of sample preparation affect the interactions of graphene with individual molecules and with bulk phases.

6.4 References

1. Shih, C.-J., Strano, M. S. & Blankschtein, D. Wetting translucency of graphene. *Nat. Mater.* **12,** 866–869 (2013).

2. Parobek, D. & Liu, H. Wettability of graphene. *2D Mater.* **2,** 32001 (2015).

3. K. S. Novoselov, S. V. Morozov, D. Jiang, Y. Zhang, S. V. Dubonos, I. V. Grigorieva, A. A. Firsov, A. K. G. Electric field effect in atomically thin carbon films. *Science* **306,** 666–669 (2004).

4. Xu, Y. *et al.* In-plane and tunneling pressure sensors based on graphene/hexagonal boron nitride heterostructures. *Appl. Phys. Lett.* **99,** 1–4 (2011).

5. Schedin, F. *et al.* Detection of individual gas molecules adsorbed on graphene. *Nat. Mater.* **6,** 652–655 (2007).

6. Heerema, S. J. & Dekker, C. Graphene nanodevices for DNA sequencing. *Nat. Nanotechnol.* **11,** 127–136 (2016).

7. Wang, Z. & Liu, C. J. Preparation and application of iron oxide/graphene based composites for electrochemical energy storage and energy conversion devices: Current status and perspective. *Nano Energy* **11,** 277–293 (2015).

8. Yoon, J. C., Yoon, C. S., Lee, J. S. & Jang, J. H. Lotus leaf-inspired CVD grown graphene for a water repellant flexible transparent electrode. *Chem. Commun.* **49,** 10626–10628 (2013).

9. Belyaeva, L. A., van Deursen, P. M. G., Barbetsea, K. I. & Schneider, G. F. Hydrophilicity of graphene in water through transparency to polar and dispersive interactions. *Adv. Mater.* **30,** 1–7 (2018).

10. Rafiee, J. *et al.* Wetting transparency of graphene. *Nat. Mater.* **11,** 217–222 (2012).

11. Taherian, F., Marcon, V., Van Der Vegt, N. F. A. & Leroy, F. What is the contact angle of water on graphene? *Langmuir* **29,** 1457–1465 (2013).

12. Wang, S., Zhang, Y., Abidi, N. & Cabrales, L. Wettability and surface free

energy of graphene films. *Langmuir* **25,** 11078–11081 (2009).

13. Driskill, J., Vanzo, D., Bratko, D. & Luzar, A. Wetting transparency of graphene in water. *J. Chem. Phys.* **141,** 18C517 (2014).

14. Shih, C. J. *et al.* Breakdown in the wetting transparency of graphene. *Phys. Rev. Lett.* **109,** 176101 (2012).

15. Ghaderi, N. & Peressi, M. First-principle study of hydroxyl functional groups on pristine, defected graphene, and graphene epoxide. *J. Phys. Chem. C* **114,** 21625–21630 (2010).

16. Li, Z. *et al.* Effect of airborne contaminants on the wettability of supported graphene and graphite. *Nat. Mater.* **12,** 925–931 (2013).

17. Yiapanis, G., Makarucha, A. J., Baldauf, J. S. & Downton, M. T. Simulations of graphitic nanoparticles at air-water interfaces. *Nanoscale* **8,** 19620–19628 (2016).

18. Andrews, J. E., Sinha, S., Chung, P. W. & Das, S. Wetting dynamics of a water nanodrop on graphene. *Phys. Chem. Chem. Phys.* **18,** 23482–23493 (2016).

19. Prydatko, A. V, Belyaeva, L. A., Jiang, L., Lima, L. M. C. & Schneider, G. F. Contact angle measurement of free-standing square-millimeter single-layer graphene. *Nat. Commun.* **9,** 4185 (2018).

20. Raj, R., Maroo, S. C. & Wang, E. N. Wettability of graphene. *Nano Lett.* **13,** 1509–1515 (2013).

21. Smith, R. S., Matthiesen, J. & Kay, B. D. Desorption kinetics of methanol, ethanol, and water from graphene. *J. Phys. Chem. A* **118,** 8242–8250 (2014).

22. Chakradhar, A. & Burghaus, U. Adsorption of water on graphene/Ru(0001)—an experimental ultra-high vacuum study. *Chem. Commun.* **50,** 7698–7701 (2014).

23. Chakradhar, A., Sivapragasam, N., Nayakasinghe, M. T. & Burghaus, U. Support effects in the adsorption of water on CVD graphene: an ultra-high vacuum adsorption study. *Chem. Commun.* **51,** 11463–11466 (2015).

24. Ceyer, S. T. New mechanisms for chemistry at surfaces. *Science* **249,** 133–139 (1990).

25. Chakradhar, A., Trettel, K. & Burghaus, U. Benzene adsorption on Ru(0001) and graphene/Ru(0001)—How to synthesize epitaxial graphene without STM or LEED? *Chem. Phys. Lett.* **590,** 146–152 (2013).

26. Chakradhar, A., Sivapragasam, N., Nayakasinghe, M. T. & Burghaus, U. Adsorption kinetics of benzene on graphene: an ultrahigh vacuum study. *J. Vac. Sci. Technol. A Vacuum, Surfaces, Film.* **34,** 21402 (2016).

27. Wehling, T. O., Lichtenstein, A. I. & Katsnelson, M. I. First-principles studies of water adsorption on graphene: the role of the substrate. *Appl. Phys. Lett.* **93,** 202110 (2008).

28. Daschbach, J. L., Peden, B. M., Smith, R. S. & Kay, B. D. Adsorption, desorption, and clustering of H_2O on Pt(111). *J. Chem. Phys.* **120,** 1516–1523 (2004).

29. Stevenson, K. P., Kimmel, G. A., Dohnálek, Z., Smith, R. S. & Kay, B. D. Controlling the morphology of amorphous solid water. *Science* **283,** 1505–1507 (1999).

30. Smith, R. S., Petrik, N. G., Kimmel, G. A. & Kay, B. D. Thermal and nonthermal physiochemical processes in nanoscale films of amorphous solid water. *Acc. Chem. Res.* **45,** 33–42 (2012).

31. Smith, R. S., Matthiesen, J., Knox, J. & Kay, B. D. Crystallization kinetics and excess free energy of H_2O and D_2O nanoscale films of amorphous solid water. *J. Phys. Chem. A* **115,** 5908–5917 (2011).

32. Gottardi, S. *et al.* Comparing graphene growth on Cu(111) versus oxidized Cu(111). *Nano Lett.* **15,** 917–922 (2015).

33. Luo, D. *et al.* Role of graphene in water-assisted oxidation of copper in relation to dry transfer of graphene. *Chem. Mater.* **29,** 4546–4556 (2017).